A diffraction problem for the biharmonic wave equation in one-dimensional periodic structures☆

Junhong Yue [a], Peijun Li [b,*], Xiaokai Yuan [c], Xiaopeng Zhu [d,e]

[a] College of Data Science, Taiyuan University of Technology, Taiyuan, Shanxi 030024, China
[b] Department of Mathematics, Purdue University, West Lafayette, IN 47907, USA
[c] School of Mathematics, Jilin University, Changchun, 130012, Jilin, China
[d] LSEC, NCMIS, ICMSEC, Academy of Mathematics and Systems Science, Chinese Academy of Sciences, Beijing 100190, China
[e] School of Mathematical Sciences, University of Chinese Academy of Sciences, Beijing 100049, China

ARTICLE INFO

ABSTRACT

This work concerns the propagation of flexural waves through one-dimensional periodic structures embedded in thin elastic plates. We show that the out-of-plane displacement of the plate only contains the Helmholtz wave component and the modified Helmholtz wave component is not supported when the Navier boundary condition is imposed. An adaptive finite element method with transparent boundary condition is developed for solving the associated boundary value problem. Numerical results show that the method is effective to solve the diffraction grating problem of the biharmonic wave equation.

1. Introduction

Diffraction gratings are optical elements with periodic structures. They have many important applications in micro-optics. An introduction to diffraction grating problems can be found in [1]. Driven by practical applications and scientific developments, this field has undergone a tremendous growth in the last several decades. We refer to [2] for a comprehensive account of mathematical and numerical studies for Maxwell's equations in periodic structures. Recently, scattering problems for biharmonic waves have played an important role in thin plate elasticity, such as the control of destructive surface waves [3,4] and the construction of ultrabroadband elastic cloaking devices [5].

Analogous to photonic and phononic crystals, periodic structures in thin elastic plates are called platonic crystals (PlaCs). Different from periodic material variations of the plate, the PlaCs can be easily fabricated by using regularly arranged arrays of cavities with any shape in the plate [6]. At the boundary of these cavities, various boundary conditions can be imposed to model different physical behavior, such as the clamped, hinged, simply supported, or free boundary condition [7]. Instead of the second-order Helmholtz equation or Maxwell's equations, the wave propagation through these structures is modeled by the fourth-order biharmonic wave equation. Although the scattering problems have been
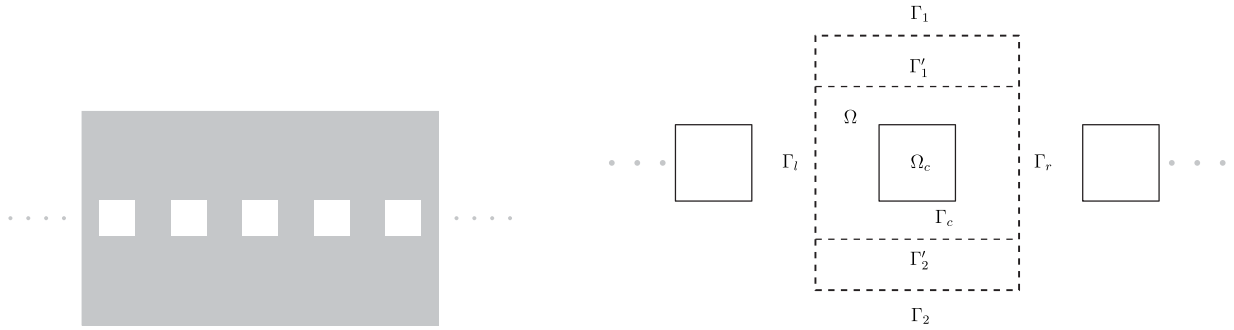
Fig. 1. Schematic of the problem geometry.

well investigated for acoustic and electromagnetic waves in periodic structures, they are much less studied for biharmonic waves and most of the available results are limited to simple and smooth geometries [8].

This paper concerns the propagation of flexural waves through one-dimensional periodic and polygonal structures embedded in thin elastic plates. In general, flexural waves contain both the Helmholtz and modified Helmholtz wave components. However, we show that only the Helmholtz wave component is sustained and the modified Helmholtz wave component is not supported when the Navier boundary condition is imposed. The Navier boundary condition arises from the hinged or Steklov boundary condition for polygonal domains [9].

Computationally, there are two challenges to solve the diffraction grating problems: the physical domains are unbounded and solutions may have local singularities. To handle these issues, effective methods were developed by combining the adaptive finite element method (FEM) and the perfect matched layer (PML) technique to solve the two- and three-dimensional problems [10–12]. Recently, an alternative approach, combining the adaptive FEM with the transparent or Dirichlet-to-Neumann (DtN) boundary condition, has been proposed to solve the scattering problems in different scenarios for acoustic, elastic, and electromagnetic waves [13–17]. This approach does not require an extra layer of artificial domain, as needed in the PML method. Based on a posteriori error estimates, the adaptive FEM algorithm was developed to refine the elements and to determine the truncation number N of the Fourier series for the DtN operator. In [18], a hybrid adaptive FEM was developed to solve the two-dimensional diffraction grating problem by combining the PML technique and the DtN operator truncation. In this work, we apply the adaptive finite element DtN method proposed in [13] to solve the associated boundary value problem for the biharmonic wave equation in one-dimensional periodic structures.

The paper is organized as follows. The model problem is introduced in Section 2. Section 3 addresses the transparent boundary condition. Section 4 discusses the grating efficiencies and the conservation of energy. The well-posedness of the associated boundary value problem is established in Section 5. Sections 6 and 7 present the adaptive FEM and numerical examples to illustrate the effectiveness of the proposed method, respectively.

2. Problem formulation

Consider a one-dimensional periodic array of rectangular holes in an infinite thin plate, as shown on the left of Fig. 1. The holes are assumed to be aligned with the x_1-axis with period Λ. Let the incident wave be a time-harmonic plane wave

$$u^{\text{inc}}(x) = e^{i(\alpha x_1 - \beta x_2)}, \quad x \in \mathbb{R}^2, \tag{2.1}$$

where $\alpha = \kappa \sin\theta$, $\beta = \kappa \cos\theta$ with $\theta \in (-\frac{\pi}{2}, \frac{\pi}{2})$ and $\kappa > 0$ being the incident angle and the wavenumber, respectively.

The problem may be restricted into a single periodic cell, as seen on the right of Fig. 1. Denote by Ω_c the hole with boundary Γ_c. Let R be a larger rectangular domain containing Ω_c. Without loss of generality, let $R = \{x \in \mathbb{R}^2 : 0 < x_1 < \Lambda, h_2 < x_2 < h_1\}$, where h_1, h_2 are constants. Define $\Gamma_j = \{x \in \mathbb{R}^2 : 0 < x_1 < \Lambda, x_2 = h_j\}, j = 1, 2$, $\Gamma_l = \{x \in \mathbb{R}^2 : x_1 = 0, h_2 < x_2 < h_1\}$, and $\Gamma_r = \{x \in \mathbb{R}^2 : x_1 = \Lambda, h_2 < x_2 < h_1\}$. Let $\Omega = R \setminus \overline{\Omega}_c$. Denote by $\Omega_1 = \{x \in \mathbb{R}^2 : 0 < x_1 < \Lambda, x_2 > h_1\}$ and $\Omega_2 = \{x \in \mathbb{R}^2 : 0 < x_1 < \Lambda, x_2 < h_2\}$ the unbounded domains above Γ_1 and below Γ_2, respectively. Let $\Gamma_j' = \{x \in \mathbb{R}^2 : 0 < x_1 < \Lambda, x_2 = h_j'\}, j = 1, 2$, where h_1', h_2' are constants satisfying $h_1' < h_1, h_2' > h_2$ such that the line segments Γ_1' and Γ_2' are above and below Ω_c, respectively.

The out-of-plane displacement of the plate u, also called the total field, satisfies the biharmonic wave equation

$$\Delta^2 u - \kappa^4 u = 0 \quad \text{in } \Omega. \tag{2.2}$$

The Navier boundary condition takes the form

$$u = \Delta u = 0 \quad \text{on } \Gamma_c. \tag{2.3}$$

Due to the periodic structure, a solution u of (2.2)–(2.3) is quasi-periodic, i.e., $u(x_1, x_2)e^{-i\alpha x_1}$ is a periodic function of x_1 with period Λ, which gives the quasi-periodic boundary condition on Γ_l and Γ_r: $u(0, x_2) = u(\Lambda, x_2)e^{-i\alpha\Lambda}$. In addition, a radiation condition is required to ensure the well-posedness of the problem: the total wave field u consists of bounded outgoing waves in Ω_1 and Ω_2 plus the incident wave u^{inc} in Ω_1.

3. Transparent boundary condition

In this section, we introduce the transparent boundary condition on $\Gamma_j, j = 1, 2$, which helps to reformulate the boundary value problem (2.2)–(2.3) from the unbounded domain into the bounded domain Ω.

Noting (2.1) and (2.2), we may verify that the diffracted field $v = u - u^{inc}$ satisfies

$$(\Delta^2 - \kappa^4)v = (\Delta - \kappa^2)(\Delta + \kappa^2)v = 0 \quad \text{in } \Omega_1.$$

Let

$$v^M = \frac{1}{2\kappa^2}\left(\Delta v + \kappa^2 v\right), \quad v^H = -\frac{1}{2\kappa^2}\left(\Delta v - \kappa^2 v\right).$$

It can be verified that the diffracted field v can be decomposed to $v = v^H + v^M$. Moreover, v^H and v^M satisfy the following Helmholtz and modified Helmholtz equations, respectively:

$$\Delta v^H + \kappa^2 v^H = 0, \quad \Delta v^M - \kappa^2 v^M = 0. \tag{3.1}$$

Hence, v^H and v^M are called the Helmholtz and modified Helmholtz wave components of v, respectively.

Using the quasi-periodicity of v^H, v^M and the radiation condition, we may solve (3.1) analytically and obtain the Rayleigh expansion for the diffracted field v in Ω_1:

$$v(x) = v^H(x) + v^M(x) = \sum_{n\in\mathbb{Z}} v_n^H(h_1)e^{i\alpha_n x_1 + i\beta_n(x_2-h_1)} + v_n^M(h_1)e^{i\alpha_n x_1 - \gamma_n(x_2-h_1)}, \tag{3.2}$$

where $v_n^H(h_1)$ and $v_n^M(h_1)$ are the Fourier coefficients of v^H and v^M on Γ_1, respectively, $\alpha_n = \alpha + n(2\pi/\Lambda)$, and

$$\gamma_n = \sqrt{\kappa^2 + \alpha_n^2}, \quad \beta_n = \begin{cases} \sqrt{\kappa^2 - \alpha_n^2} & \text{for } |\alpha_n| < \kappa, \\ i\sqrt{\alpha_n^2 - \kappa^2} & \text{for } |\alpha_n| > \kappa. \end{cases}$$

The Rayleigh expansion (3.2) shows that v^H consists of both the propagating and evanescent plane waves, while v^M is made of only the evanescent plane waves. Taking the Laplacian on both sides of (3.2) and using (3.1), we get

$$\Delta v = \Delta v^H + \Delta v^M = \kappa^2(-v^H + v^M)$$
$$= \sum_{n\in\mathbb{Z}} -\kappa^2 v_n^H(h_1)e^{i\alpha_n x_1 + i\beta_n(x_2-h_1)} + \kappa^2 v_n^M(h_1)e^{i\alpha_n x_1 - \gamma_n(x_2-h_1)}. \tag{3.3}$$

Assume that v and Δv are given on Γ_1. Due to the quasi-periodicity, they have the Fourier expansions

$$v(x_1, h_1) = \sum_{n\in\mathbb{Z}} v_n(h_1)e^{i\alpha_n x_1}, \quad \Delta v(x_1, h_1) = \sum_{n\in\mathbb{Z}} (\Delta v)_n(h_1)e^{i\alpha_n x_1}. \tag{3.4}$$

Evaluating (3.2)–(3.3) on Γ_1 and using (3.4), we have from a straightforward calculation that

$$v_n^H(h_1) = \frac{1}{2}\left(v_n(h_1) - \frac{1}{\kappa^2}(\Delta v)_n(h_1)\right), \quad v_n^M(h_1) = \frac{1}{2}\left(v_n(h_1) + \frac{1}{\kappa^2}(\Delta v)_n(h_1)\right).$$

Substituting $v_n^H(h_1), v_n^M(h_1)$ into the normal derivatives of (3.2) and (3.3) on Γ_1 leads to

$$\partial_{\nu_1} v(x_1, h_1) = \sum_{n\in\mathbb{Z}} \left(\frac{1}{2}(i\beta_n - \gamma_n)v_n(h_1) - \frac{1}{2\kappa^2}(i\beta_n + \gamma_n)(\Delta v)_n(h_1)\right)e^{i\alpha_n x_1},$$
$$\partial_{\nu_1} \Delta v(x_1, h_1) = \sum_{n\in\mathbb{Z}} \left(-\frac{\kappa^2}{2}(i\beta_n + \gamma_n)v_n(h_1) + \frac{1}{2}(i\beta_n - \gamma_n)(\Delta v)_n(h_1)\right)e^{i\alpha_n x_1}, \tag{3.5}$$

where $\nu_1 = (0, 1)$ is the unit outward normal vector to Γ_1.

Define two Dirichlet-to-Neumann (DtN) operators

$$(T_1 f)(x_1) = \sum_{n\in\mathbb{Z}} i\beta_n f_n e^{i\alpha_n x_1}, \quad (T_2 f)(x_1) = \sum_{n\in\mathbb{Z}} \gamma_n f_n e^{i\alpha_n x_1}, \tag{3.6}$$

where f_n are the Fourier coefficients of f. By (3.5), the following transparent boundary condition (TBC) can be imposed for the total field u on Γ_1:

$$\partial_{\nu_1} u = \frac{1}{2}(T_1 - T_2)u - \frac{1}{2\kappa^2}(T_1 + T_2)\Delta u + g_1, \quad \partial_{\nu_1}\Delta u = -\frac{\kappa^2}{2}(T_1 + T_2)u + \frac{1}{2}(T_1 - T_2)\Delta u + g_2, \tag{3.7}$$

where $g_1(x_1) = -2i\beta e^{i(\alpha x_1 - \beta h_1)}$ and $g_2(x_1) = 2i\beta\kappa^2 e^{i(\alpha x_1 - \beta h_1)}$.

Similarly, we may deduce the Rayleigh expansion for the total field u in Ω_2:

$$u(x) = u^{\mathrm{H}}(x) + u^{\mathrm{M}}(x) = \sum_{n \in \mathbb{Z}} u_n^{\mathrm{H}}(h_2)e^{i\alpha_n x_1 - i\beta_n(x_2 - h_2)} + u_n^{\mathrm{M}}(h_2)e^{i\alpha_n x_1 + \gamma_n(x_2 - h_2)}. \tag{3.8}$$

The TBC for the total field u on Γ_2 is given by

$$\partial_{\nu_2} u = \frac{1}{2}(T_1 - T_2)u - \frac{1}{2\kappa^2}(T_1 + T_2)\Delta u, \quad \partial_{\nu_2}\Delta u = -\frac{\kappa^2}{2}(T_1 + T_2)u + \frac{1}{2}(T_1 - T_2)\Delta u, \tag{3.9}$$

where $\nu_2 = (0, -1)$ is the unit outward normal vector to Γ_2.

4. Grating efficiencies

In this section, we discuss the grating efficiencies and show a simple but important result on the conservation of energy. It states that the incident energy is equal to the total energy of the diffracted and transmitted wave components.

Lemma 4.1. *Assume that u is a quasi-periodic function satisfying*

$$\begin{cases} \Delta^2 u - \kappa^4 u = 0 & \text{in } \Omega, \\ u = \Delta u = 0 & \text{on } \Gamma_c. \end{cases} \tag{4.1}$$

Then

$$\Im \int_{\Gamma_1 \cup \Gamma_2} (\bar{u}\partial_\nu \Delta u - \Delta u \overline{\partial_\nu u})ds = 0. \tag{4.2}$$

Proof. Since κ is a real number, the complex conjugate of u also satisfies (4.1). Using the integral identity

$$\int_\Omega (v\Delta^2 u - u\Delta^2 v)dx = \oint_{\partial\Omega} (v\partial_\nu \Delta u - \Delta u\partial_\nu v)ds - \oint_{\partial\Omega} (u\partial_\nu \Delta v - \Delta v\partial_\nu u)ds,$$

we take $v = \bar{u}$ and obtain

$$\oint_{\partial\Omega} (\bar{u}\partial_\nu \Delta u - \Delta u\overline{\partial_\nu u})ds - \oint_{\partial\Omega} (u\overline{\partial_\nu \Delta u} - \Delta\bar{u}\partial_\nu u)ds = 0,$$

where $\partial\Omega = \Gamma_c \cup \Gamma_l \cup \Gamma_r \cup \Gamma_1 \cup \Gamma_2$.

It follows from the Navier boundary condition that

$$\int_{\Gamma_c} (\bar{u}\partial_\nu \Delta u - \Delta u\overline{\partial_\nu u})ds - \int_{\Gamma_c} (u\overline{\partial_\nu \Delta u} - \Delta\bar{u}\partial_\nu u)ds = 0.$$

Since u is a quasi-periodic function, Δu and $\partial_{x_1} u$ are also quasi-periodic functions, which imply

$$\int_{\Gamma_l \cup \Gamma_r} (\bar{u}\partial_\nu \Delta u - \Delta u\overline{\partial_\nu u})ds - \int_{\Gamma_l \cup \Gamma_r} (u\overline{\partial_\nu \Delta u} - \Delta\bar{u}\partial_\nu u)ds = 0.$$

The proof is completed by combining the above equations. $\square$

It follows from the biharmonic wave Eq. (2.2) that u admits the decomposition

$$u = u^{\mathrm{H}} + u^{\mathrm{M}} \quad \text{in } \Omega_j, \tag{4.3}$$

where

$$u^{\mathrm{H}} = u^{\mathrm{inc}} + v^{\mathrm{H}}, \quad u^{\mathrm{M}} = v^{\mathrm{M}} \quad \text{in } \Omega_1.$$

Moreover, u^{H} and u^{M} satisfy the Helmholtz and modified Helmholtz equations, respectively. Substituting (4.3) into (4.2), we obtain from a simple calculation that

$$\Im \int_{\Gamma_1 \cup \Gamma_2} \left(u^{\mathrm{H}}\overline{\partial_\nu u^{\mathrm{H}}} - u^{\mathrm{M}}\overline{\partial_\nu u^{\mathrm{M}}}\right)ds = 0. \tag{4.4}$$

Define $U = \{n \in \mathbb{Z} : |\alpha_n| < \kappa\}$. Let

$$r_n = \left(\frac{\beta_n}{\beta}\right)|v_n^{\mathrm{H}}(h_1)|^2, \quad t_n = \left(\frac{\beta_n}{\beta}\right)|u_n^{\mathrm{H}}(h_2)|^2, \quad n \in U,$$

where r_n and t_n are called the nth order diffracted and transmitted efficiencies, respectively.

Theorem 4.2. *Let r_n and t_n be the nth order diffracted and transmitted efficiencies. Then*

$$\sum_{n \in U}(r_n + t_n) = 1.$$

Proof. By Rayleigh's expansion (3.2), we have on Γ_1 that

$$u^{\mathrm{H}} = u^{\mathrm{inc}} + v^{\mathrm{H}} = e^{\mathrm{i}(\alpha x_1 - \beta h_1)} + \sum_{n \in \mathbb{Z}} v_n^{\mathrm{H}}(h_1)e^{\mathrm{i}\alpha_n x_1},$$

$$\partial_{\nu_1} u^{\mathrm{H}} = \partial_{x_2} u^{\mathrm{inc}} + \partial_{x_2} v^{\mathrm{H}} = -\mathrm{i}\beta e^{\mathrm{i}(\alpha x_1 - \beta h_1)} + \sum_{n \in \mathbb{Z}} \mathrm{i}\beta_n v_n^{\mathrm{H}}(h_1)e^{\mathrm{i}\alpha_n x_1},$$

$$u^{\mathrm{M}} = v^{\mathrm{M}} = \sum_{n \in \mathbb{Z}} v_n^{\mathrm{M}}(h_1)e^{\mathrm{i}\alpha_n x_1}, \quad \partial_{\nu_1} u^{\mathrm{M}} = \partial_{x_2} v^{\mathrm{M}} = -\sum_{n \in \mathbb{Z}} \gamma_n v_n^{\mathrm{M}}(h_1)e^{\mathrm{i}\alpha_n x_1}.$$

Similarly, we get from Rayleigh's expansion (3.8) on Γ_2 that

$$u^{\mathrm{H}} = \sum_{n \in \mathbb{Z}} u_n^{\mathrm{H}}(h_2)e^{\mathrm{i}\alpha_n x_1}, \quad \partial_{\nu_2} u^{\mathrm{H}} = -\partial_{x_2} u^{\mathrm{H}} = \sum_{n \in \mathbb{Z}} \mathrm{i}\beta_n u_n^{\mathrm{H}}(h_2)e^{\mathrm{i}\alpha_n x_1},$$

$$u^{\mathrm{M}} = \sum_{n \in \mathbb{Z}} u_n^{\mathrm{M}}(h_2)e^{\mathrm{i}\alpha_n x_1}, \quad \partial_{\nu_2} u^{\mathrm{M}} = -\partial_{x_2} u^{\mathrm{M}} = -\sum_{n \in \mathbb{Z}} \gamma_n u_n^{\mathrm{M}}(h_2)e^{\mathrm{i}\alpha_n x_1}.$$

Substituting the above expansions into (4.4) and the orthogonality of the exponential functions, we obtain

$$\Im \int_{\Gamma_1 \cup \Gamma_2} \left(u^{\mathrm{H}}\overline{\partial_\nu u^{\mathrm{H}}} - u^{\mathrm{M}}\overline{\partial_\nu u^{\mathrm{M}}}\right)ds = \mathrm{i}\beta\Lambda - \sum_{n \in U}\mathrm{i}\beta_n\Lambda|v_n^{\mathrm{H}}(h_1)|^2 - \sum_{n \in U}\mathrm{i}\beta_n\Lambda|u_n^{\mathrm{H}}(h_2)|^2 = 0,$$

which completes the proof. □

It is clear to note from (4.3) and Theorem 4.2 that the energy comes from the propagating modes of the Helmholtz wave component and the modified Helmholtz wave component does not carry energy and makes no contribution to the energy conservation.

5. The well-posedness

This section is to address the well-posedness of the associated boundary value problem. Consider two auxiliary functions

$$p = \Delta u - \kappa^2 u, \quad q = \Delta u + \kappa^2 u. \tag{5.1}$$

Clearly, p and q are also quasi-periodic functions. It is easy to note from (2.2) that p and q satisfy the Helmholtz and modified Helmholtz equations, respectively. Moreover, it is easy to verify

$$u = \frac{1}{2\kappa^2}(q - p), \quad \Delta u = \frac{1}{2}(q + p), \tag{5.2}$$

and

$$p = -2\kappa^2 u^{\mathrm{H}}, \quad q = 2\kappa^2 u^{\mathrm{M}}, \tag{5.3}$$

where u^{H} and u^{M} are the Helmholtz and modified Helmholtz wave components of u, respectively.

It follows from (5.1)–(5.2), the Navier boundary condition (2.3), and the TBCs (3.7) and (3.9) that p and q satisfy the following boundary value problems:

$$\begin{cases} \Delta p + \kappa^2 p = 0 & \text{in } \Omega, \\ p = 0 & \text{on } \Gamma_c, \\ \partial_{\nu_1} p = T_1 p + g_3 & \text{on } \Gamma_1, \\ \partial_{\nu_2} p = T_1 p & \text{on } \Gamma_2, \end{cases} \tag{5.4}$$

and

$$\begin{cases} \Delta q - \kappa^2 q = 0 & \text{in } \Omega, \\ q = 0 & \text{on } \Gamma_c, \\ \partial_{\nu_1} q = -T_2 q & \text{on } \Gamma_1, \\ \partial_{\nu_2} q = -T_2 q & \text{on } \Gamma_2, \end{cases} \tag{5.5}$$

where $g_3 = g_2 - \kappa^2 g_1 = 4\mathrm{i}\beta\kappa^2 e^{\mathrm{i}(\alpha x_1 - \beta h_1)}$.

The well-posedness of (5.4) can be established by following a similar proof of [2, Theorem 3.5]. The details are omitted for brevity.

Theorem 5.1. *For all but possibly a discrete set of wavenumbers κ, the boundary value problem (5.4) admits a unique weak solution $p \in H^1_{c,qp}(\Omega) = \{u \in H^1(\Omega) : u(0, x_2) = u(\Lambda, x_2)e^{-i\alpha\Lambda}$ and $u = 0$ on $\Gamma_c\}$.*

Theorem 5.2. *The boundary value problem (5.5) has only a trivial solution, i.e., $q = 0$.*

Proof. Consider the variational formulation of (5.5): find $q \in H^1_{c,qp}(\Omega)$ such that

$$\int_\Omega \nabla q \cdot \nabla\overline{\phi}dx + \kappa^2 \int_\Omega q\overline{\phi}dx + \sum_{j=1}^2 \int_{\Gamma_j} (T_2 q)\overline{\phi}ds = 0 \quad \forall \phi \in H^1_{c,qp}(\Omega).$$

The continuity of the DtN operator T_2 can be similarly shown by following [2, Lemma 3.3]. Hence it suffices to show that the sesquilinear form is coercive.

A simple calculation yields

$$\int_\Omega |\nabla q|^2 dx + \kappa^2 \int_\Omega |q|^2 dx + \sum_{j=1}^2 \int_{\Gamma_j} (T_2 q)\overline{q}ds$$

$$= \|\nabla q\|^2_{L^2(\Omega)} + \kappa^2 \|q\|^2_{L^2(\Omega)} + \Lambda \sum_{j=1}^2 \sum_{n \in \mathbb{Z}} (\kappa^2 + \alpha_n^2)^{1/2} |q_n|^2 \geq C\|q\|^2_{H^1(\Omega)},$$

where C is a positive constant. The proof is completed by applying the Lax–Milgram lemma. $\square$

Combining (5.3) and Theorem 5.2, we conclude that the wave field u only contains the Helmholtz wave component u^H and does not sustain the modified Helmholtz wave component u^M, which is also consistent with the conservation of energy discussed in Section 4.

6. The adaptive finite element method

In this section, we briefly present the adaptive finite element DtN method to solve the model problem (2.2)–(2.3). The detail of the method can be found in [13]. By (5.1)–(5.5) and Theorem 5.2, it suffices to solve the boundary value problem (5.4).

First the DtN operator defined in (3.6) needs to be truncated to a summation of finitely many terms

$$(T_{1,N}f)(x_1) = \sum_{|n| \leq N} i\beta_n f_n e^{i\alpha_n x_1}, \tag{6.1}$$

where the truncation number N is a positive integer. The variational problem with the truncated DtN operator is to find $p_N \in H^1_{c,qp}(\Omega)$ such that

$$b_N(p_N, v) = \int_{\Gamma_1} g_3 \overline{v}ds \quad \forall v \in H^1_{c,qp}(\Omega), \tag{6.2}$$

where the sesquilinear form $b_N : H^1_{c,qp}(\Omega) \times H^1_{c,qp}(\Omega) \to \mathbb{C}$ is given by

$$b_N(u, v) = \int_\Omega \nabla u \cdot \nabla\overline{v}dx - \kappa^2 \int_\Omega u\overline{v}dx - \sum_{j=1}^2 \int_{\Gamma_j} (T_{1,N}u)\overline{v}ds = \int_{\Gamma_1} g_3 \overline{v}ds.$$

Denote by $\mathcal{M}_h$ a regular triangulation of the domain Ω, where h stands for the maximum diameter of the triangles in $\mathcal{M}_h$. To enforce the quasi-periodic boundary condition, it is required that if $(0, x_2)$ is a nodal point on Γ_l, then (Λ, x_2) should also be a nodal point on Γ_r, and vice versa.

Let $V_h \subset H^1_{qp}(\Omega) = \{u \in H^1(\Omega) : u(0, x_2) = u(\Lambda, x_2)e^{-i\alpha\Lambda}\}$ be the usual piecewise polynomial finite element space satisfying the quasi-periodic boundary condition, i.e.,

$$V_h := \left\{v \in C(\overline{\Omega}) : v|_K \in P_m(K) \ \forall K \in \mathcal{M}_h, v(0, x_2) = e^{-i\alpha\Lambda}v(\Lambda, x_2)\right\},$$

where $m > 0$ is an integer and $P_m(K)$ is the set of all polynomials of degrees no more than m. The finite element approximation to (6.2) is to find p_N^h with $p_N^h = 0$ on Γ_c such that

$$b_N(p_N^h, v^h) = \int_{\Gamma_1} g_3 \overline{v^h}ds \quad \forall v^h \in V_{h,c}, \tag{6.3}$$

where $V_{h,c} = \{v \in V_h : v = 0 \text{ on } \Gamma_c\}$.

It follows from [19] that the discrete inf-sup condition of the sesquilinear form b_N holds for sufficiently large N and sufficiently small h. The general theory in [20] may be employed to show that the truncated variational problem (6.3) has a unique solution $p_N^h \in V_{h,c}$.

Table 1

The adaptive finite element algorithm.

(1) Given a threshold $\tau \in (0, 1)$ and a prescribed tolerance $\epsilon > 0$;
(2) Choose h_1 and h_2 to fix the computational domain Ω;
(3) Choose N and h'_1, h'_2 such that the truncation error $\epsilon_N \leq 10^{-8}$;
(4) Generate a triangulation $\mathcal{M}_h$ over Ω and compute η_K and ϵ_h;
(5) If $\epsilon_h > \epsilon$, then
(6)   Refine the element $\hat{K} \in \mathcal{M}_h$ if $\eta_{\hat{K}} > \tau \max\limits_{K \in \mathcal{M}_h} \eta_K$;
(7)   Solve the discrete problem (6.3) on the new mesh $\mathcal{M}_h$;
(8)   Compute η_K and ϵ_h on the new mesh $\mathcal{M}_h$;
(9) End if.

For any triangular element $K \in \mathcal{M}_h$, let h_K be its diameter. Denote by $\mathcal{B}_h$ the set of all the edges of K. For any edge $e \in \mathcal{B}_h$, let h_e be its length. If e is the interior edge of the common side of K_1 and $K_2 \in \mathcal{M}_h$, then we define the jump residual across e by

$$J_e = \nabla p_N^h|_{K_1} \cdot \nu_1 + \nabla p_N^h|_{K_2} \cdot \nu_2,$$

where ν_j is the unit normal vector on the boundary of $K_j, j = 1, 2$.

If $e \subset \Gamma_1$ and $e' \subset \Gamma_2$ are boundary edges, then we define the jump residual

$$J_e = 2\left(\partial_{\nu_1} p_N^h|_K - T_{1,N} p_N^h|_K - g_3\right), \quad J_{e'} = 2\left(\partial_{\nu_2} p_N^h|_K - T_{1,N} p_N^h|_K\right).$$

For any boundary edge on the left boundary Γ_l, i.e., $e \in \{x_1 = 0\} \cap \partial K_1$ for some $K_1 \in \mathcal{M}_h$, and its corresponding edge on the right boundary $e' \in \{x_2 = \Lambda\} \cap \partial K_2$ for some $K_2 \in \mathcal{M}_h$, the jump residual is

$$J_e = \partial_{x_1} p_N^h|_{K_1} - e^{-i\alpha\Lambda}\partial_{x_1} p_N^h|_{K_2}, \quad J_{e'} = e^{i\alpha\Lambda}\partial_{x_1} p_N^h|_{K_1} - \partial_{x_1} p_N^h|_{K_2}.$$

For any triangular element $K \in \mathcal{M}_h$, we define the local error estimator

$$\eta_K = h_K \|\mathscr{R} p_N^h\|_{L^2(K)} + \left(\frac{1}{2}\sum_{e \in \partial K} h_e \|J_e\|^2_{L^2(e)}\right)^{1/2},$$

where $\mathscr{R}$ is the residual operator given by

$$\mathscr{R}u = \Delta u + \kappa^2 u.$$

The following a posteriori error estimate is proved in [13].

Theorem 6.1. *Let p and p_N^h be the solutions of* (5.4) *and* (6.3)*, respectively. Then there exists a positive integer N_0 independent of h and satisfying $(2\pi N_0/\Lambda)^2 > \kappa^2$ such that for $N \geq N_0$ the following a posteriori error estimate holds:*

$$\|p - p_N^h\|_{H^1(\Omega)} \leq C\left(\left(\sum_{K \in \mathcal{M}_h} \eta_K^2\right)^{1/2} + \sum_{j=1}^2 e^{-|h_j - h'_j|\sqrt{(2\pi N/\Lambda)^2 - \kappa^2}}\right),$$

where the constant $C > 0$ is independent of h and N.

7. Numerical experiments

It can be seen from Theorem 6.1 that the a posteriori error contains the finite element discretization error ϵ_h and the truncation error of the DtN operator ϵ_N. More precisely, we have

$$\epsilon_h = \left(\sum_{K \in \mathcal{M}_h} \eta_K^2\right)^{1/2}, \quad \epsilon_N = e^{-|h_j - h'_j|\sqrt{(2\pi N/\Lambda)^2 - \kappa^2}}.$$

Table 1 describes the adaptive finite element DtN algorithm which was originally developed in [13]. The algorithm is implemented by using FreeFem [21] with more accurate quadratic elements, i.e., $m = 2$, instead of the first order linear elements adopted in [13]. Next we present some numerical examples to demonstrate the competitive performance of the method.
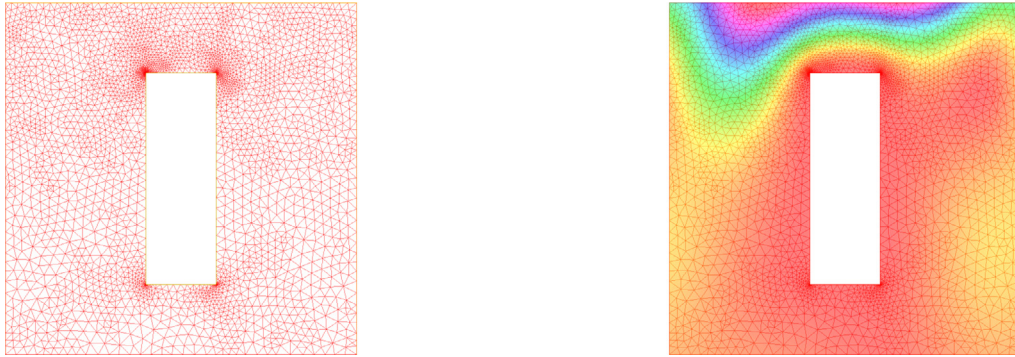
Fig. 2. Example 1: (left) the adaptively refined mesh; (right) the magnitude of the corresponding solution.
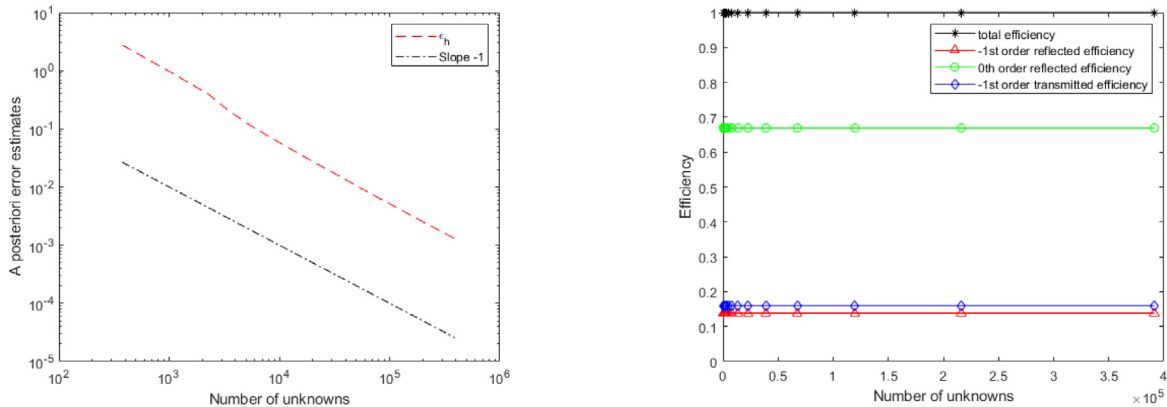

Fig. 3. Example 1: (left) the convergent rate; (right) the grating efficiencies.

7.1. Example 1: one rectangular hole

In one period, the hole is a rectangle centered at origin with the width $w = 0.2$ and the height $h = 0.6$, as seen in Fig. 2. Let the period $\Lambda = 1$ and the constants $h_1 = 0.5$, $h_2 = -0.5$. The incident angle is $\theta = \pi/3$ and the wavenumber is $\kappa = 2\pi$, which is equivalent to the wavelength $\lambda = 1$. The DtN operator truncation number is $N = 13$. The solution has local singularities at the four vertexes of the rectangle. Fig. 2 shows the adaptively refined mesh after seven iterations with the number of nodal points $n = 3542$ and the magnitude of the corresponding solution. Clearly, the method captures the feature of the solution and adaptively refines the mesh around the four vertexes of the rectangle. The a posteriori error estimate and grating efficiencies of the diffracted field and transmitted field are shown in Fig. 3. It can be seen that the rate of convergence is quasi-optimal, i.e., the second order of convergence, and the conservation of energy is confirmed. Table 2 shows the negative first order (R_{-1}) and the zeroth order (R_0) diffracted efficiencies computed by using the uniform and adaptive meshes. It is clear to note that the results computed under the uniform mesh with the number of unknowns or the degree of freedom (DoF) 608882 is quite similar to the one computed under the adaptive mesh with the number of unknowns 8225, which shows the superior performance of the adaptive method.

7.2. Example 2: two rectangular holes

In this example, we present the numerical results for the structure with two rectangular holes. Let the period $\Lambda = 1$ and the constants $h_1 = 0.5$, $h_2 = -0.5$. The width and height of each rectangular hole are $w = 0.2$, $h = 0.6$, and the two holes are separated with a distance 0.1, as seen in Fig. 4. The incident angle is $\theta = \pi/3$, the wavenumber is $\kappa = 2\pi$, and the DtN operator truncation number is $N = 13$. Fig. 4 shows the refined mesh after 7 iterations with the number of nodal points $n = 9479$ and the magnitude of the corresponding solution. It is clear to see that the method yields finer meshes around the eight vertexes where the solution has singularities and generates coarse meshes at other places where the solution is smooth. The a posteriori error estimate and grating efficiencies of the diffracted field and transmitted field are plotted in Fig. 5, which show the quasi-optimal convergence and the conservation of energy.

Table 2
Example 1: The diffracted efficiencies computed by using the adaptive and uniform meshes.

| Adaptive mesh				Uniform mesh			
k	DoF_h	R_{-1}	R_0	k	DoF_h	R_{-1}	R_0
0	376	0.1382451	0.6705408707	0	376	0.1382451	0.6705408707
1	750	0.1406306699	0.66689113	1	1544	0.1387493508	0.6687997504
2	1356	0.1387930824	0.6690532288	2	9602	0.1386819178	0.6690925316
3	2259	0.1386933111	0.6691748615	3	40098	0.1386309501	0.669175853
4	3356	0.1386281602	0.6692123118	4	152646	0.1386092285	0.6692087059
5	5001	0.1386079011	0.6692244345	5	421868	0.1386086723	0.6692181011
6	8225	0.1386038417	0.6692274714	6	608882	0.138605332	0.6692198291
7	13798	0.1386030692	0.6692281415				
8	22694	0.1386027564	0.6692283448				
9	38994	0.138602683	0.6692283957				
10	67565	0.1386026677	0.6692284049				
11	119780	0.1386026595	0.6692284096				
12	216195	0.1386026581	0.6692284103				
13	391325	0.1386026577	0.6692284104				
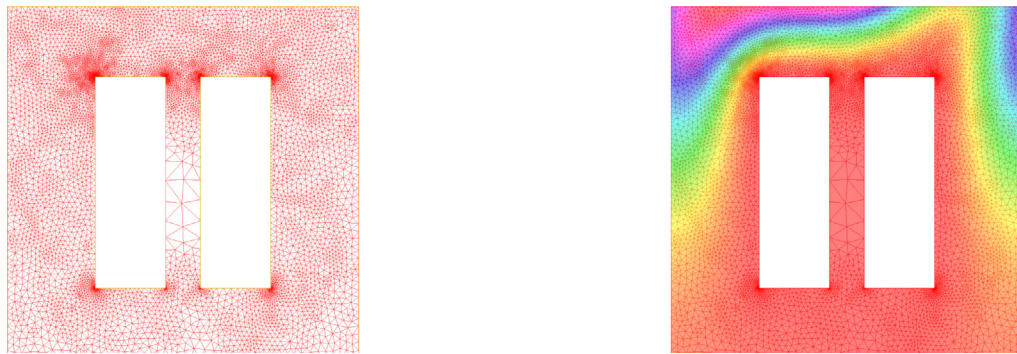
Fig. 4. Example 2: (left) the adaptively refined mesh; (right) the magnitude of the corresponding solution.
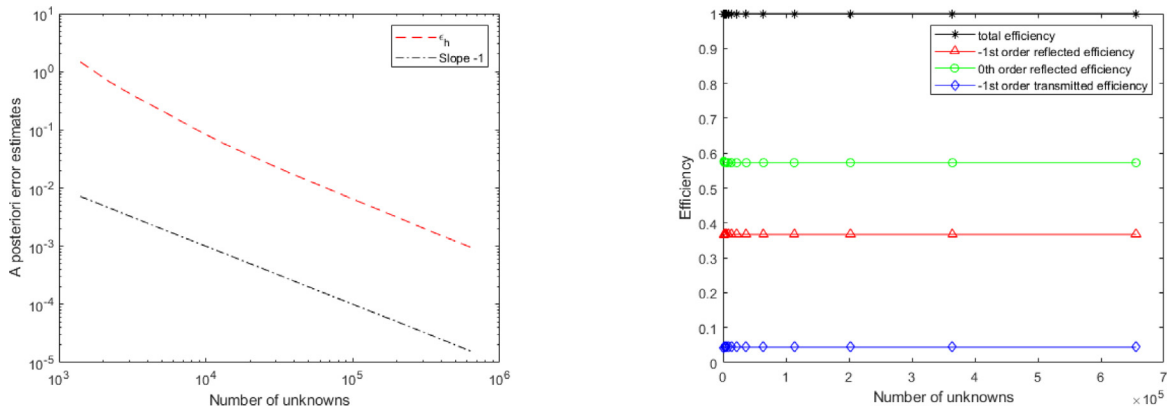

Fig. 5. Example 2: (left) the convergent rate; (right) the grating efficiencies.

7.3. Example 3: two triangular holes

In this example, we test the structure with two triangular holes with two vertexes closely pointing to each other. The solution has higher singularities than the previous two examples. The period and constants of the domain Ω are the same as Examples 1 and 2, i.e., $\Lambda = 1$ and $h_1 = 0.5, h_2 = -0.5$. The coordinates of three vertexes on each triangle is $(0.15, \pm 0.3), (0.49, 0)$ and $(0.85, \pm 0.3), (0.51, 0)$. The incident angle is $\theta = \pi/3$ and the wavenumber is $\kappa = 2\pi$. Fig. 6 shows the refined mesh with the number of nodal points 5141 and the magnitude of the corresponding solution after seven iterations. To resolve the singularity of the solution, the mesh is much finer around the vertexes, especially around the two close vertexes. The a posteriori error estimate and grating efficiencies of the diffracted field and transmitted field are plotted in Fig. 7. The quasi-optimal convergence and the conservation of energy are observed. As a comparison, Table 3
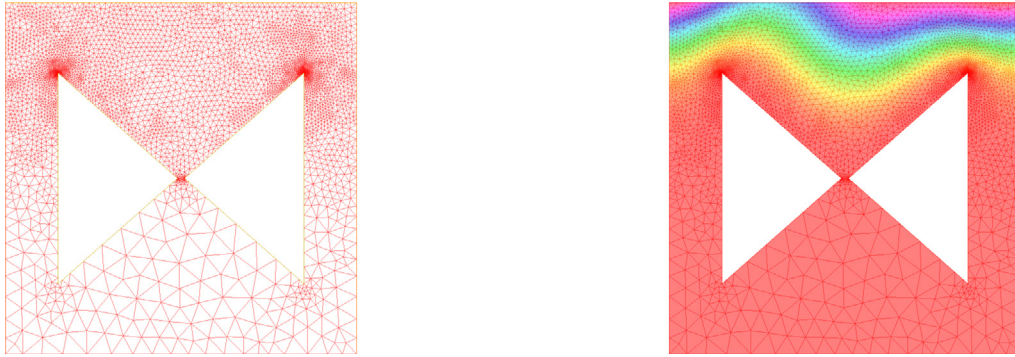
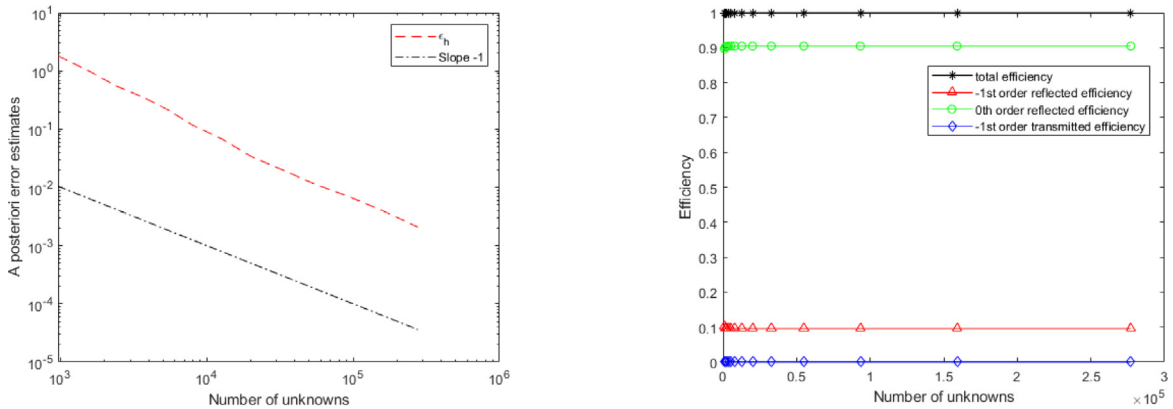**Fig. 6.** Example 3: (left) the adaptively refined mesh; (right) the magnitude of the corresponding solution.

Fig. 7. Example 3: (left) the convergent rate; (right) the grating efficiencies.

Table 3
Example 3: The diffracted efficiencies computed by using the adaptive and uniform meshes.

Adaptive mesh				Uniform mesh			
k	DoF_h	R_{-1}	R_0	k	DoF_h	R_{-1}	R_0
0	961	0.1034999785	0.8964969217	0	961	0.1034999785	0.8964969217
1	1559	0.09792189298	0.9020748196	1	2815	0.09963449174	0.9003621062
2	2409	0.09617564786	0.9038209822	2	10495	0.09748482119	0.9025116032
3	3769	0.09565098829	0.9043456059	3	23547	0.09666973828	0.9033266315
4	5466	0.09546812455	0.9045284646	4	48055	0.09630595447	0.9036903851
5	7934	0.09541092934	0.904585617	5	264271	0.09570326818	0.9042930272
6	12766	0.09539261972	0.9046037955	6	598323	0.09561823779	0.9043780496
7	20087	0.09538715201	0.9046091727				
8	32842	0.09538557897	0.9046107106				
9	54905	0.09538509332	0.9046111833				
10	93372	0.0953849428	0.9046113298				
11	159058	0.0953848892	0.9046113819				
12	277050	0.09538487338	0.9046113973				

gives the negative first order (R_{-1}) and the zeroth order (R_0) diffracted efficiencies computed by the adaptive and uniform meshes. Once again, it shows that the adaptive method yields better numerical results than the uniform mesh.

8. Conclusion

We have presented an adaptive finite element DtN method for solving the biharmonic plate wave equation in one-dimensional periodic structures. Based on the TBC and two auxiliary functions, the underlying boundary value problem is reformulated equivalently into two decoupled boundary value problems in a bounded domain, which are used to show that the flexural wave only contains the Helmholtz wave component. The a posteriori error estimate based adaptive finite element DtN method is adopted to solve the discrete problem with the truncated DtN operator. Numerical results show

that the method is effective to resolve the problems with singular solutions. Future work includes extending the method to solve the problems with other boundary conditions.

Declaration of competing interest

The authors declare that they have no known competing financial interests or personal relationships that could have appeared to influence the work reported in this paper.

Data availability

Data will be made available on request.

References

[1] Petit R, editor. Electromagnetic theory of gratings. In: Topics in current physics. Vol. 22. Berlin, Heidelberg: Springer; 1980.
[2] Bao G, Li P. Maxwell's equations in periodic structures. Series on applied mathematical sciences, vol. 208, Singapore: Springer; 2022.
[3] Watanabe E, Utsunomiya T, Wang CM. Hydroelastic analysis of pontoon-type VLFS: a literature survey. Eng Struct 2004;6:245–56.
[4] Evans DV, Porter R. Penetration of flexural waves through a periodically constrained thin elastic plate in vacuo and floating on water. J Engrg Math 2007;58:317–37.
[5] Farhat M, Guenneau S, Enoch S. Ultrabroadband elastic cloaking in thin plates. Phys Rev Lett 2009;103:024301.
[6] McPhedran RC, Movchan AB, Movchan NV. Platonic crystals: Bloch bands, neutrality and defects. Mech Mater 2009;41:356–63.
[7] Gazzola F, Grunau H-C, Sweers G. Polyharmonic boundary value problems: positivity preserving and nonlinear higher order elliptic equations in bounded domains. In: Lecture notes in mathematics, Berlin, Heidelberg: Springer; vol. 1991.
[8] Smith MJA. Wave propagation through periodic structures in thin plates (Ph.D. thesis), The University of Auckland; 2013.
[9] Destuynder Ph, Salaun M. Mathematical analysis of thin plate models, mathématiques & applications. Vol. 24. Berlin, Heidelberg: Springer; 1996.
[10] Chen Z, Wu H. An adaptive finite element method with perfectly matched absorbing layers for the wave scattering by periodic structures. SIAM J Numer Anal 2003;41:799–826.
[11] Bao G, Chen Z, Wu H. Adaptive finite element method for diffraction gratings. J Opt Soc Amer A 2005;22:1106–14.
[12] Bao G, Li P, Wu H. An adaptive edge element method with perfectly matched absorbing layers for wave scattering by periodic structures. Math Comp 2010;79:1–34.
[13] Wang Z, Bao G, Li J, Li P, Wu H. An adaptive finite element method for the diffraction grating problem with transparent boundary condition. SIAM J Numer Anal 2015;53:1585–607.
[14] Jiang X, Li P, Lv J, Zheng W. An adaptive finite element method for the wave scattering with transparent boundary condition. J Sci Comput 2017;72:936–56.
[15] Jiang X, Li P, Lv J, Wang Z, Wu H, Zheng W. An adaptive finite element DtN method for Maxwell's equations in biperiodic structures. IMA J Numer Anal 2022;42:2794–828.
[16] Li P, Yuan X. Convergence of an adaptive finite element DtN method for the elastic wave scattering by periodic structures. Comput Methods Appl Mech Engrg 2020;360:112722.
[17] Li P, Yuan X. An adaptive finite element DtN method for the elastic wave scattering problem. Numer Math 2022;150:993–1033.
[18] Zhou W, Wu H. An adaptive finite element method for the diffraction grating problem with PML and few-mode DtN truncations. J Sci Comput 2018;76:1813–38.
[19] Schatz AH. An observation concerning Ritz–Galerkin methods with indefinite bilinear forms. Math Comp 1974;28:959–62.
[20] Babuška I, Aziz A. Survey lectures on mathematical foundations of the finite element method. In: Aziz A, editor. The mathematical foundation of the finite element method with application to the partial differential equations. New York: Academic Press; 1973, p. 5–359.
[21] Hecht F. New development in FreeFem++. J Numer Math 2012;20:251–65.